

The SOFIA Telescope in Full Operation

Andreas Reinacher^{1,2,5}, Friederike Graf^{1,3}, Benjamin Greiner¹,
Holger Jakob^{1,2}, Yannick Lammen^{1,2}, Sarah Peter^{1,2},
Manuel Wiedemann^{1,3}, Oliver Zeile^{1,2} and Hans J. Kaercher⁴

¹Deutsches SOFIA Institut, University of Stuttgart
Pfaffenwaldring 29, 70569 Stuttgart, Germany

²SOFIA Airborne Systems Operations Center
NASA Armstrong Flight Research Center
Mail Stop DAOF S241, P. O. Box 273
Edwards CA 93523, USA

³SOFIA Science Center, NASA Ames Research Center
Mail Stop N-211-1, Moffett Field CA 94035, USA

⁴MT Mechatronics, Weberstrasse 21
55130 Mainz, Germany

⁵reinacher@dsi.uni-stuttgart.de

Received April 14, 2018; Accepted July 4, 2018; Published August 27, 2018

The SOFIA telescope is a 2.5 m class Cassegrain telescope with Nasmyth focus. It is the largest telescope ever integrated into an aircraft. The telescope is exposed to the stratospheric environment during the observations and the fact that the telescope's foundation, which is a Boeing 747 SP, is vibrating and moving in all degrees of freedom (DoF) requires a highly specialized and sophisticated design. Based on the telescope of its predecessor, the Kuiper Airborne Observatory (KAO), the SOFIA telescope design had to evolve to accommodate a telescope 2.5 times the size of KAO. In several hundred successful observation flights, the telescope proved that it performs not only as specified, but is also extremely reliable. Nevertheless, the telescope's software and hardware are continuously upgraded to optimize its performance without interfering with the observation schedules to reach even more ambitious image size and pointing jitter goals to enable additional science cases. In addition, manufacturing of the line-replaceable units is in process to ensure that the SOFIA telescope can perform without any major interruptions for the envisioned 20 year lifetime. Some of the main features of the SOFIA telescope are its suspension assembly (SUA), which decouples the telescope from SOFIA's fuselage with air springs and a spherical oil bearing, the extremely stiff Nasmyth tube (NT), which connects cavity and cabin mounted components of the dumbbell design, and the Secondary Mirror Assembly (SMA), which is used for chopping and fast pointing corrections. This paper aims to give an overview of these and all other major telescope subsystems in operation today. In addition, some of the upgrades, either implemented recently or slated for implementation shortly, are introduced.

Keywords: SOFIA, telescope, optical assembly, suspension assembly, mass dampers, imager, pointing control.

1. Introduction

The Stratospheric Observatory For Infrared Astronomy (SOFIA) is a 2.5 m class flying observatory designed for operating in a large wavelength band of 0.3 μm –1.6 mm. It operates at altitudes of 35,000–45,000 ft, above 99% of the atmosphere's water

vapor content. Before the start of the observations, a large sliding door is opened to reveal a 5.5×4.1 m opening in the aft fuselage so that the telescope has an unobstructed view of the night sky. Figure 1 shows SOFIA in flight with the telescope visible in the aft part of the fuselage.



Fig. 1. SOFIA during a rare daytime test flight with the open cavity door in the aft fuselage. The telescope mirrors were protected with covers for these initial envelope expansion flights that were performed to proof the structural integrity of the fuselage after the extensive modifications.

In addition to the airframe vibrations, opening of the door also exposes the telescope to significant aerodynamic excitations, pressures of approx. 0.2 bar and temperatures of -40°C . Ensuring stable telescope pointing under these extreme conditions was the major design driver for the consortium of the two German companies MAN (now MT Mechatronics) and Kayser-Threde (now part of OHB System AG) that designed and built the telescope on behalf of the German Aerospace Center DLR. Out of the long list of requirements, two of the most challenging to meet were:

- (1) Point-source images in wavelengths of $5\text{--}10\ \mu\text{m}$ shall have a diameter corresponding to 50% encircled energy of less than 3.8 arcsec.
- (2) Point-source images in wavelengths of $50\ \mu\text{m}$ or more shall have a diameter corresponding to 50% encircled energy of less than the wavelength in microns divided by 9.4. *This requirement ensures diffraction-limited images at wavelengths $\geq 50\ \mu\text{m}$.*

Both requirements are defined for exposure times of at least one second at an altitude of at least 41,000 feet. To give the various science instruments significant performance or efficiency enhancements and even enable additional science cases requiring high-spatial resolution in the mid-infrared wavelengths, the SOFIA program works towards meeting even more challenging goals of 1.8 instead of 3.8 arcsec image diameter for the shorter wavelengths and diffraction-limited images at wavelengths $\geq 25\ \mu\text{m}$. The translation of these goals into image jitter and

SOFIA's currently achieved performance are detailed in [Graf et al. \(2018a\)](#) and are not part of this paper. This paper is intended to provide a comprehensive description of the SOFIA telescope and its major subsystems as it is in almost daily operation today.

The partially disassembled telescope was shipped to Waco, Texas, in 2002 for integration into the SOFIA aircraft on L3-Communications Integrated System premises. A first on-sky test was performed in 2004. While the aircraft modifications were being completed, DLR contracted the University of Stuttgart, which founded the Deutsches SOFIA Institut (DSI), to commission, maintain and further develop the telescope. The next major milestones were SOFIA's first flight in 2007, and the first telescope activations in flight, with closed cavity door later in 2007 and open cavity door in 2010. 14 years after those initial on-sky tests, the telescope nowadays is operated four nights a week, demonstrating very high reliability and performance ([Temi et al., 2014](#)).

Different aspects of the SOFIA telescope have been described in several publications, mainly during its assembly and integration phase from around 2000 to 2004, e.g. [Stoeffler & Heydenreich \(2000\)](#); [Erdmann et al. \(2000\)](#); [Sust et al. \(2003\)](#); [Wandner \(2003\)](#); [Bittner et al. \(2004\)](#). In the following years, a number of improvements to parts of the system done by DSI were also described in various conference papers; summaries are provided in [Wolf et al. \(2016\)](#) and [Reinacher et al. \(2016a\)](#).

In Sec. 2, some general telescope facts are given, followed by a description of the telescope optics, i.e.

Primary and Tertiary Mirror with their suspensions and the active Secondary Mirror with its drive unit. Also part of the telescope optics are the three optical cameras Focal Plane Imager (FPI), Fine Field Imager (FFI), and Wide Field Imager (WFI). They are used for target acquisition and guiding and are described in Sec. 2.4.

Then the Suspension Assembly (SUA), which enables the telescope to steadily point at a target despite the numerous disturbances acting on its structure, is described in Sec. 3. It consists of the Vibration Isolation System, which decouples the translational degrees of freedom (DOF) of the telescope from the aircraft, and the Rotations Isolation Assembly, which does the same for the rotational DOF. The drive units, Coarse Drive, Fine Drive and Balancer Drive, used for pointing and balancing the telescope are also described in the SUA section.

In Sec. 4, the Tracker, which uses images acquired with one of the three guide cameras to track on a target, and a brief summary of ongoing improvement work to this system are introduced. Due to the nature of the disturbance environment, tracking is not sufficient to keep the telescope pointed on the target. Therefore, the required higher frequency pointing towards control loop is then described in Sec. 5 before the summary.

2. General Telescope Design and Optical Assembly

Due to the limited space available in the fuselage of a Boeing 747, a Cassegrain reflector with Nasmyth

focus was the chosen configuration for the SOFIA telescope. Just like in the KAO, SOFIA's predecessor, the telescope optics are exposed to the stratosphere during operations, while the science instrument is located in the heated and pressurized aircraft cabin. This allows the scientists on board to access their instrument, even in flight.

As detailed in [Kaercher et al. \(2014, 2016\)](#), there were several design concepts investigated in the design phase. In the end, a dumbbell design with the telescope supported in the pressure bulkhead between the cabin and open port cavity prevailed. While this may not be the optimal solution from a structural mechanics point of view, it simplifies the aircraft/telescope interface.

Figure 2 shows a sectional cut of the telescope suspended in the pressure bulkhead, which separates the Telescope Assembly (TA) cavity exposed to the stratosphere during observations and the heated and pressurized cabin. From this figure, it is obvious that the telescope is part of the pressure and temperature boundary, as well. Figure 3 illustrates a CAD model of the telescope and gives the location of some of the described subsystems.

To minimize the deformation of the "dumbbell" through gravity loads, a very stiff connection between the cavity side optics and the cabin side instrument flange was required. This so-called Nasmyth tube (NT) shown in Fig. 4 in the manufacturing phase at MAN Technologie (now MT Aerospace) in Augsburg, Germany, is made from carbon fiber reinforced polymer (CFRP). Its wall thickness is 30 mm and it weighs about 700 kg. The NT is extremely stiff and by

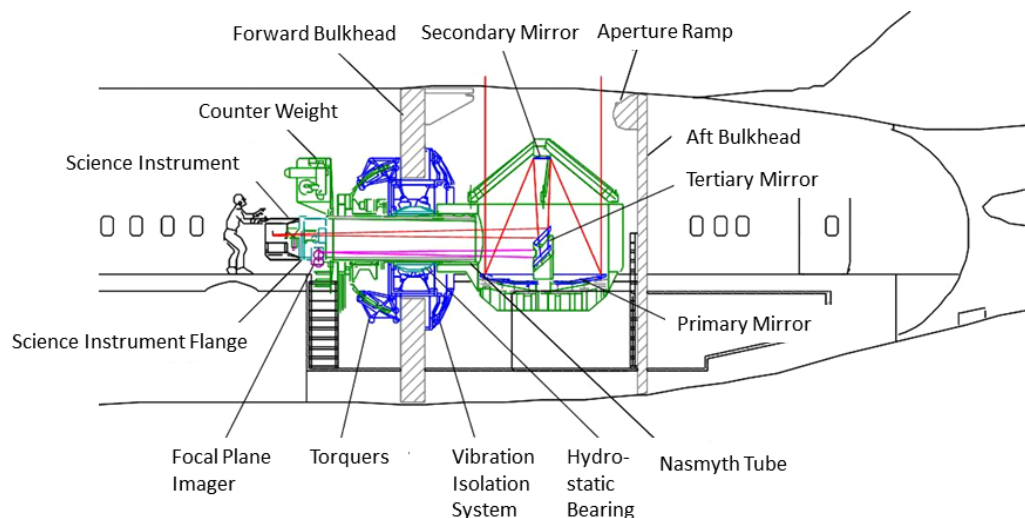


Fig. 2. Sectional schematic of the telescope in the airframe with the aircraft cabin to the left and the telescope cavity to the right of the additionally installed bulkhead. Bulkhead and telescope act as temperature and pressure barrier between the two segments.

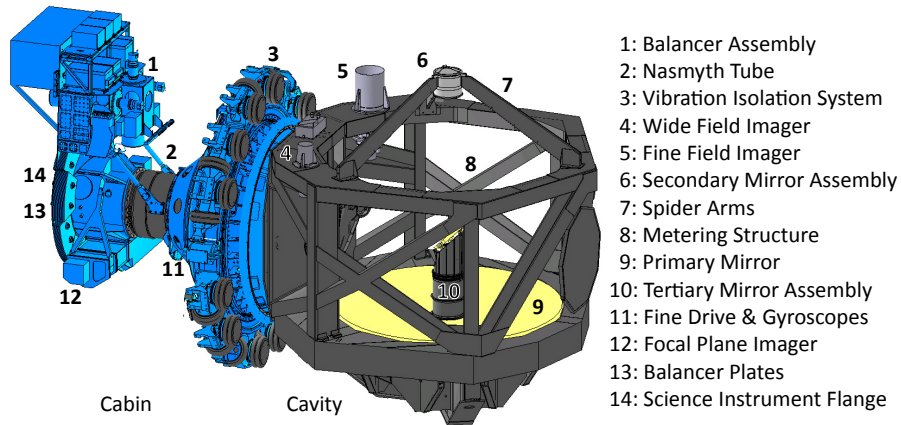


Fig. 3. The SOFIA telescope with some of the described subsystems.

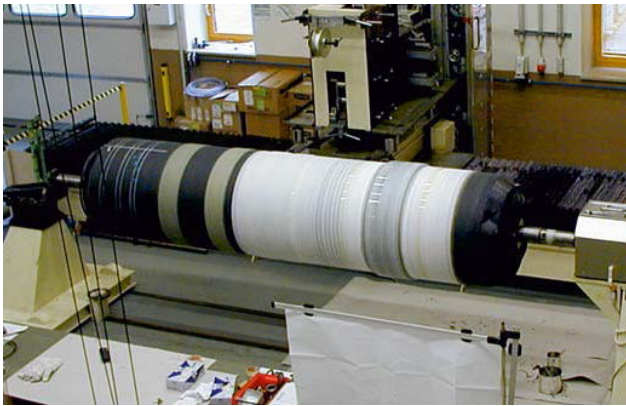


Fig. 4. The NT in a late manufacturing stage.

choosing the right combination of carbon fiber and resin, the coefficient of thermal expansion (CTE) is on the order of only a few percent of the CTE of steel. This is of great importance for the application in SOFIA because the NT experiences a large temperature difference between its two ends. The cabin-side end is held at room temperature, while the cavity side cools down to about -40°C in flight.

The telescope tube is an open lattice work, also made of CFRP. So is the mirror cell, which provides an isostatic support for the Primary Mirror (PM), and the telescope spider arms, which hold the Secondary Mirror Assembly (SMA) in its place above the PM.

2.1. Primary mirror assembly

SOFIA's light collecting PM has a parabolic shape with a diameter of 2.7 m with an effective aperture of 2.5 m and a f-number of $f/1.28$. The mirror is made of Zerodur, a special glass ceramic made by

Schott, with an extremely low coefficient of thermal expansion (CTE) of about $0.1 \cdot 10^{-6}\text{K}^{-1}$ or less. This allows to maintain the shape of the mirror surface within SOFIA's operating temperature range between room temperature at the ground and about -40°C during observation flights. After casting, the monolithic mirror body weighed about 3.5 t but was then polished and light weighted by the French company REOSC down to approximately 900 kg by milling and etching a ribbed structure with hexagonal pockets into the backside of the mirror body.

Figure 5 shows the PM without coating with a light source placed behind the mirror to visualize the light weighting. The Tertiary Mirror with its support structure is visible in the center. The load of the mirror weight is supported by 18 evenly distributed axial pads which are connected to steel rods on a whiffletree support structure (Fig. 6).

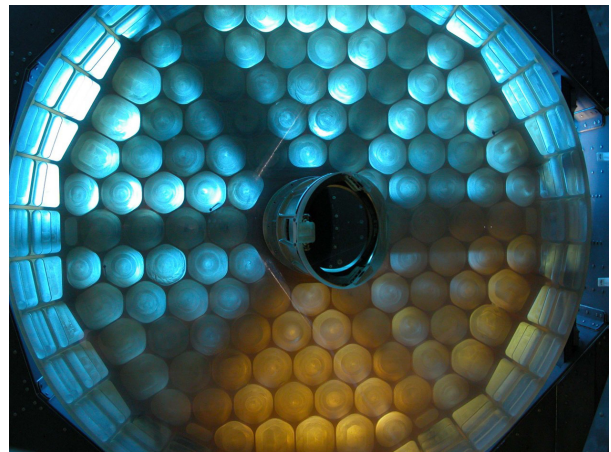


Fig. 5. The light weighted PM before coating with the Tertiary Mirror Assembly (TMA) visible in the center.

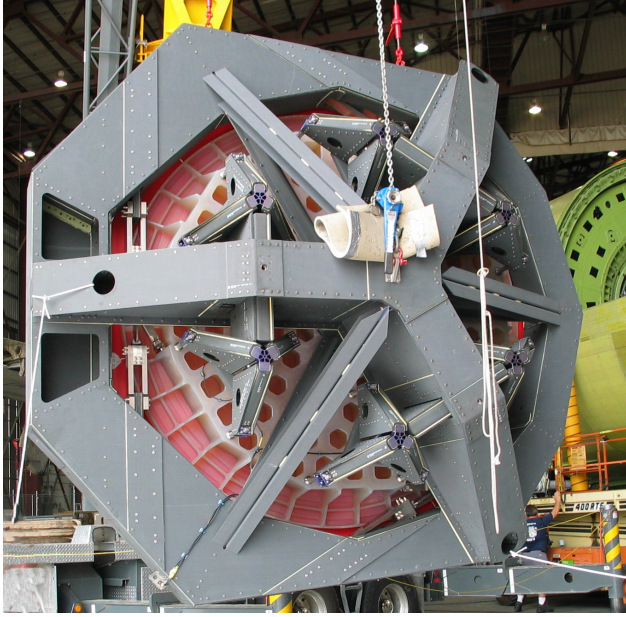


Fig. 6. The PMA before integration into the aircraft.

Flexible metallic hinges within these rods ensure that only axial forces are transferred. A separate lateral support structure with steel cantilever springs holds the mirror at three points from the side. Both the axial and the lateral support, are embedded in a carbon fiber structure, the so-called PM Cell. As the CTE of Zerodur is significantly different from the CTE of the carbon fiber panels of the support structure and the CTE of the steel of the support rods and springs, the design includes thermal compensation features comprised of Invar and steel blocks. These features decouple the temperature dependent deformation of the support structure from the mirror body, minimizing the constraint forces that would deform the mirror surface.

The PM Cell has precisely specified interface points to the TA Metering Structure and the NT. This makes it possible to detach the whole Primary Mirror Assembly (PMA) from the telescope structure, hoist it out of the aircraft and renew the 150 nm thick pure aluminum coating in SOFIA's mirror coating facility (Ali *et al.*, 2018). Originally, it was planned to execute such a re-coating every other year. However, frequently performed reflectivity tests of the PM show surprisingly little degradation, enabling the delay of this time-consuming process to a degree that it had not to be performed to this date.

As SOFIA's telescope structure is subject to high dynamic loads from aircraft motion and

turbulence, the characterization of the dynamic properties of the structure was always in the focus during the design and integration phase. After manufacturing of the PMA but before integration into the TA and into the aircraft, the PMA was subject to a dedicated modal survey test, which characterized the eigenfrequencies and mode shapes of SOFIA's largest optical unit.

After integration into the aircraft, characterization during test flights continued and the structure was equipped with sensors (accelerometers, thermocouples, pressure sensors). This included sensors are directly attached to the backside of the PM. After about 65 temperature cycles (= open door flights), it was discovered that the aluminum tie-downs and the strong epoxy (3M Scotch-Weld DP490) used to attach the cabling of the sensors caused small cracks in the Zerodur because of the large differences in CTE. After a thorough investigation, all tie-downs were removed and all fractures were erased by grinding. Only a very limited number of sensors and their cables were re-attached with a much improved method, using aluminum tape and Invar tie-downs. The now smaller set of sensors is about to be used during regular science flights by being integrated into the active control system for the telescope attitude and image jitter correction (see Sec. 5).

2.2. Secondary mirror assembly

2.2.1. Secondary mirror

Signal-to-noise ratios in infrared observing can be as low as 1/100,000, i.e. the target's signal can only be extracted from the various sources of background (e.g. atmospheric emission, thermal emission from telescope and science instrument) by using a range of observation techniques. The main background source, the atmospheric emission, is often determined and subsequently eliminated from the data by tilting SOFIA's Secondary Mirror (SM or M2) such that the telescope points to an area on the sky close to the target that does not contain another infrared source. This technique is called chopping. Since the atmospheric emission can change rapidly, typical chop frequencies on SOFIA are 2–5 Hz, i.e. there are 4–10 transitions between the two SM positions per second.

Following such a square wave pattern exerts the SM to high dynamic loads. To minimize the resulting deformation of the SM's optical surface, it

is made from Silicon Carbide with a very high Young modulus of 420 GPa. Manufactured by the ASTRUM/BOOSTEC joint venture SiCSPACE, almost pure SiC powder (98.5%) was sintered to form so-called S-SiC (Fruit et al., 2003). To reduce scatter, the hyperbolic convex optical surface was then coated with a thin layer of SiC CVD before polishing. Finally, a pure Aluminum coating was applied to achieve high reflectivity values.

With a lightweight back structure, the 352 mm mirror weighs less than 2 kg and has a very low moment of inertia of $0.015 \text{ kg} \cdot \text{m}^2$ and because of its high stiffness, a first eigenfrequency was formed beyond 2 kHz. A central cut-out with a diameter of 40 mm is used to mount the obscuration stop, also called Secondary Mirror Button.

The mirror is attached to the Secondary Mirror Mechanism (SMM) via three flexure-type bipods that prevent the introduction of forces through the differing CTE's of SiC and the aluminum of the mirror cell. The SMM was built by the Swiss company CSEM and is made up of two subsystems, the Tilt Chop Mechanism (TCM) and the Focus Center Mechanism (FCM). All the three subsystems together are called SMA and are shown in Fig. 7.

2.2.2. Tilt chop mechanism

The TCM's main purpose is to perform infrared chopping, i.e. it can be tilted such that its angular

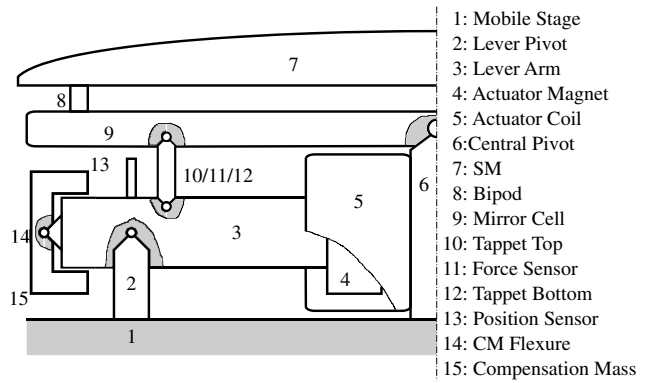


Fig. 8. Schematics of the TCM that illustrates the reaction force compensated design that moves a compensation mass in the opposite angular direction of the mirror movement.

position follows a square wave with a frequency of up to 20 Hz and a peak amplitude of up to 1125 arcsec for symmetric chops around the center position, which translates into a chop throw of 10 arcmin on the sky. The direction of the chop can be chosen arbitrarily. It is a reaction force compensated design, i.e. the large and abrupt movements of the TCM do not transmit into the telescope structure. This was realized by using lever arms to transmit the motion of the motors to the mirror cell and a ring shaped compensation mass simultaneously. As illustrated in Fig. 8, this results in the angular deflection of the mirror cell/mirror assembly and the deflection of the compensation mass in the opposing angular direction. Three of the linear motors are arranged in a 120° pattern around the center (see Fig. 7). All moving parts are guided by flexures to avoid backlash and friction and also to provide stiffness against wind loads. Position feedback is provided by three eddy current displacement sensors.

During initial telescope on sky testing in 2004, it became apparent that the TCM resonated with a frequency of approximately 300 Hz. Unfortunately, this vibration caused sizable image smear in the focal plane. While initial FEA models did not indicate a structural resonance at this frequency, it turned out that the PID-type control algorithm was part of the problem.

Consequently, the TCM controller is one of the areas that underwent major improvements after its delivery and integration into the telescope (Reinacher, 2014; Reinacher et al., 2010, 2011, 2016b). The PID controller was replaced with a pole placement controller that was designed such that the closed loop system poles match those of a Bessel

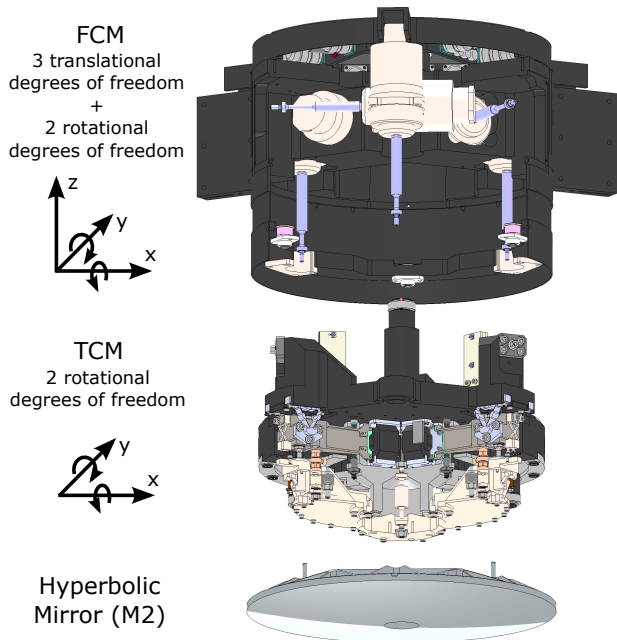


Fig. 7. Exploded view of the three parts of SOFIA's SMA.

filter to guarantee optimal square wave behavior. Two issues, a delay in the position feedback and high position sensor noise, were successfully addressed by implementing a Kalman filter. Non-linear dependencies on temperature and amplitude were also modeled and are included in the real-time state estimation. These modifications led to a significantly improved position stability of the SM, which is located in close proximity to the cavity opening and therefore subject to significant aerodynamic loads. The transitions time between two chop positions is 10 ms for all amplitudes.

Further improvements, however, are still restricted by the structural frequency at 300 Hz, which in the meantime was identified with a more detailed FEA model as a structural mode of the compensation mass.

Apart from chopping, the TCM's purpose is to act as actuator for fast image motion corrections with a bandwidth of approximately 50 Hz and peak amplitudes of 11 arcsec on the sky. Since there are a number of telescope vibrations modes beyond 50 Hz that negatively affect the telescope jitter performance, there is currently an effort underway to damp or eliminate the 300 Hz mode through minimal but very specific hardware modifications. Test runs performed with a prototype indicate a possible extension of the bandwidth to approx. 90 Hz. For more information, please refer to [Lammen *et al.* \(2018\)](#).

Furthermore, there are already preliminary studies and proof-of-concept type hardware mock-ups in place to improve the bandwidth even further through the addition of a piezo actuator driven stage between TCM and Secondary Mirror.

An aircraft maintenance period in 2014 was used to take down the SMA from the telescope to perform a thorough inspection. The TCM was partially taken apart to get access to all flexures for inspection but no major corrosion or wear and tear were discovered ([Lammen *et al.*, 2016](#)).

2.2.3. Focus center mechanism

The TCM is attached to the FCM, which is the interface to the telescope structure, namely the three spider arms. It consists of a hexapod with six custom-made actuators with brushless motors and a high friction gear assembly for high stiffness and accuracy. It has a range of ± 3 mm in lateral direction, ± 5 mm in focus direction and a tip/tilt range of 1125 arcsec.

The FCM is used to bring the SM into collimation and to adjust the telescope focus. While re-collimation is only required when a component in the optical path was replaced or adjusted, focusing must be done frequently, especially at the beginning of SOFIA observations when the telescope cools down from ground to stratospheric temperatures. An empirical relationship between the SMA temperature and the optimal focus position has been established and is used for automated focus adjustments.

In addition to establishing collimation, FCM tip/tilt deflections are also used to increase the amplitude of asymmetric chops. Asymmetric chops are patterns with one chop position in the SM center position to avoid coma, which is introduced by large deflections of the SM.

2.3. Tertiary mirror assembly

The TMA consists of two flat mirrors attached to an Invar structure that fold the incoming light through the NT to the detectors on the cabin side. Both mirrors are elliptical with a size of approximately 480 mm \times 350 mm. The first tertiary mirror in the optical path (TM-1) is made from Herasil, a fused Silica material, with a dichroic gold coating. It reflects the infrared part of the light ($> 90\%$ reflectivity for wavelengths $> 2 \mu\text{m}$) to the science instrument, but has high transmissivity at shorter wavelengths (> 0.5 for wavelengths between 480 and 800 nm). This visible part of the light is then reflected by the second tertiary mirror (TM-2), which is a protected silver coated Zerodur mirror, to SOFIA's main guide camera, the FPI.

2.4. Acquisition and guide cameras

There are three acquisition and guide cameras on SOFIA that operate in the VIS/NIR spectrum (wavelength range: ~ 350 – 1000 nm):

- (1) The FPI, which uses the telescope optics and is the main guide camera. During regular observations the FPI is used for tracking, i.e. the acquired images are used to determine centroid positions that are then used to send pointing corrections to the attitude control system.
- (2) The FFI, which is located on the telescope hearing (see [Fig. 3](#)). With its larger field of view (FoV), it is used for acquisition and as backup tracking camera for occasions where there is no visible source close enough to the infrared target to be available in the FPI.

- (3) The WFI with yet a larger FoV to allow for easier star pattern recognition is used for target acquisition.

Having three cameras also gives the observatory some redundancy: In case one camera fails during a mission, the observations can be completed with the remaining two cameras in most cases.

2.4.1. Focal plane imager

The FPI is located on the temperature-controlled cabin side of the telescope and is an on-axis guide camera that covers the FoV of each science instrument. The FPI has a large achromat and re-imaging lens that reduces the telescope's focal length of $f \approx 49,140$ mm to $f \approx 5,240$ mm, giving it a focal ratio of $f/2.1$. Its FoV encompasses nearly the entire unvignetted imaging area of the SOFIA telescope, which has about 9 arcmin diameter. It is the most sensitive of the three guide cameras, due to the size of the optics, and has the highest spatial resolution with ~ 0.51 arcsec/pixel. It is also the only guide camera that sees any movements of the chopping SM and can be used to verify focus of the SI.

The original FPI sensor had 1024×1024 pixels with a pixel pitch of $14 \mu\text{m}$. The frame transfer architecture allowed operation without a mechanical shutter and a duty cycle of nearly 100% in the parallel readout mode. The sensor was an uncooled, front-illuminated CCD with a peak quantum efficiency of 19%. In early 2013, the camera was replaced with a commercial off-the-shelf camera (Andor iXon 888). The new sensor also has a 1024×1024 pixel imaging area with slightly smaller $13 \mu\text{m}$ pixels and frame transfer architecture. It features a back-illuminated EMCCD detector and a thermoelectric cooler, capable of cooling the sensor to 100 K below ambient. The new camera, dubbed FPI+, has a peak quantum efficiency of 94% and 5 orders of magnitude lower dark current rate than the original camera. This increased the sensitivity by a factor of 100, or 5 stellar magnitudes, allowing the FPI+ tracking on stars as faint as $V = 16$ mag with an exposure time of 3 s (without chopping).

The FPI+ has a double filter wheel, where one wheel is equipped with a Sloan spectral filter set (u' , g' , r' , i' , and z') and the second wheel with three neutral density filters (ODs 1.3, 2.6, and 4.0), a 950 nm cut-on filter used for daylight tracking, and a blocking position. Since its integration, the FPI+ has also become an official science instrument that is

offered in SOFIA's call for proposals and has since been used for various stellar occultation and exoplanet transit observations (Pfüller et al., 2018).

2.4.2. Fine field imager

The FFI is a 254 mm Schmidt–Cassegrain telescope with a focal reducer to achieve a focal ratio of $f/2.9$. This gives it a 67×67 arcmin FoV. The FFI is mounted to the main telescope's heading on the cavity side and is therefore exposed directly to stratospheric conditions in flight. The FFI is designed as a secondary guide camera and is usually used when there is no suitable guide star in the FFI's smaller FoV. To track on very bright stars, a set of three neutral density filters is available and a 950 nm cut-on filter for daylight tracking. The FFI optics are designed to be in focus, both on ground and during flight, without the need of a focuser. However, during the transient conditions shortly after the cavity door opens at the beginning of the flight, the FFI is significantly out of focus, due to the inhomogeneous cool-down of the FFI's PM. Due to its shape, which is significantly thinner on the outside than on the inside, and the relatively high CTE of the Borosilicate glass ($\approx 3.2 \times 10^{-6} \text{ K}^{-1}$), the PM's curvature radius decreases until thermal equilibrium is reached (see Fig. 9). While the FFI is out of focus in the first ~ 2 h of flight, its sensitivity and centroid accuracy are significantly reduced.

The FFI still is equipped with the same sensor as the original FPI. To improve its sensitivity and to mitigate the defocusing issue at the beginning of the flight, DSI is working on upgrading the optics and the camera. The new FFI+ optics will be a 300 mm $f/2.2$ Riccardi–Honders telescope, designed and built by Officina Stellare. All its optical elements are made from fused silica with a low CTE of $\approx 0.3 \times 10^{-6} \text{ K}^{-1}$. The thickness of the large front lens and the Mangin mirror (a lens with an aluminized backside, designed to eliminate spherical aberrations of conventional mirrors) is nearly

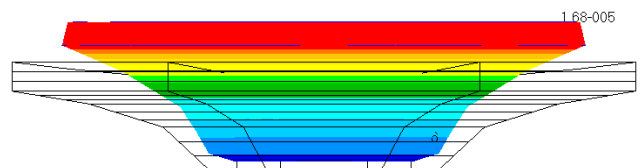


Fig. 9. (Color online) The finite element analysis shows that the original FFI's PM changes its curvature radius during cool-down (colored shape). Once thermal equilibrium is reached, the mirror returns to its original shape (white shape).

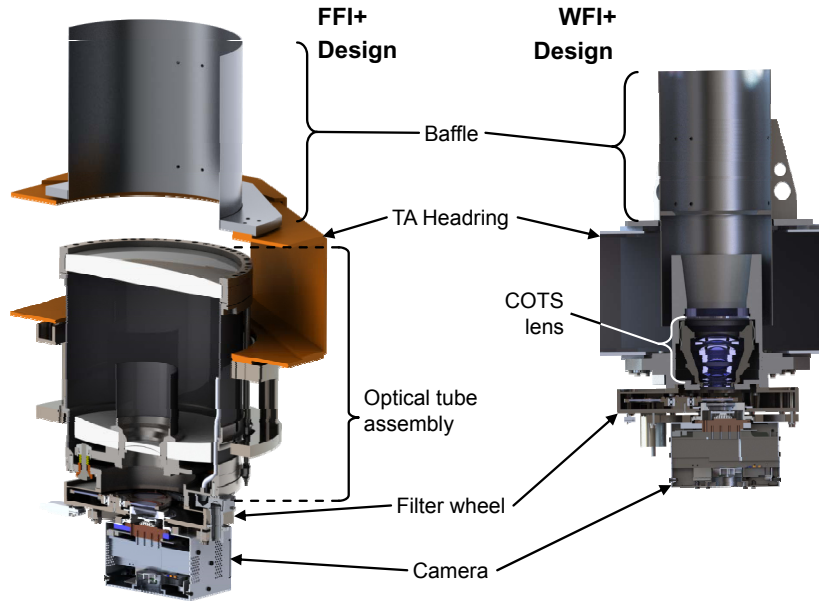


Fig. 10. Design of the new FFI+ (left) and WFI+ (right).

constant over the radius, which will allow it to cool more homogeneously and achieve a much more stable focus, even during the cool-down phase of the telescope.

The new camera is a ruggedized version of the Andor iXon 888 camera, so it can withstand stratospheric conditions and is described in detail in [Wiedemann *et al.* \(2016\)](#). The design of the new FFI+ is shown in Fig. 10. With the new larger optics and the more sensitive detector, the new FFI+ will be able to track on $V = 13$ mag stars and fainter.

2.4.3. Wide field imager

The WFI is a 68 mm aperture Petzval lens with a focal ratio of $f/2.0$. It has a large $6^\circ \times 6^\circ$ FoV and is primarily used for target acquisition. It has the same filter set available as the FFI. Since the WFI also suffers from the relatively poor sensitivity of the original cameras, it too will be upgraded with a new optics and camera. It was decided to test several commercial off-the-shelf lenses to find a lens that can retain a stable focus during conditions on the ground as well as in flight (without mechanically adjusting the focus). Out of several candidates a Canon Cine lens with $f = 85$ mm and $T/1.3$ was selected ([Lachenmann *et al.*, 2014](#)). Coupled with the same camera that will be used for the FFI+, it will be sensitive to stars of at least $V = 11$ mag. Its design is shown on the right in Fig. 10. Planned integration of both FFI+ and WFI+ is early 2019.

3. Suspension Assembly

Arguably the most challenging part of an airborne telescope is stabilizing the observed target in the focal plane despite the many disturbances acting on the observatory. Vibrations of the jet engines and turbulence excite the aircraft fuselage and aerodynamic and aero-acoustic excitations act directly on the exposed telescope structure and optics in the cavity.

A multi-layered approach to isolate the telescope from these disturbances and enable inertial stabilization of the telescope was taken by the TA Consortium. When the telescope is ready for observations, there is no rigid connection to the aircraft fuselage. Instead, the telescope floats on the air springs and dampers of the Vibration Isolation System (VIS). The decoupling from aircraft roll, pitch and yaw is realized with a hydrostatic bearing, the so-called Rotation Isolation Assembly (RIA). The inertial attitude of the telescope is sensed with fiber optic gyroscopes and actively controlled with the Coarse Drive (CD) and Fine Drive (FD) Assemblies.

The dumbbell design requires a good balance between the telescope optics in the cavity and the science instrument on the cabin side. Coarse balancing to adjust to the difference in mass between the various instruments is done by adding or removing steel plates at the Balancing Flange on the cabin side. To compensate for the boil off of the cryogenics used to cool down the infrared detectors in

flight, the Balancer Drive Assembly is actuated to move a steel mass with constant, very low speed away from the telescope's center of gravity.

The images taken with the cameras described in Sec. 2.4 are used for actively tracking on a visible target, while a compensation for image motion caused by flexible telescope bending is derived from accelerations measurements of the telescope structure (see Sec. 5).

3.1. Vibration isolation system

The VIS serves two purposes:

- (1) During observations it isolates the telescope from high frequency vibrations caused by the airplane's engines and aero-elastic deformations of the wings and control surfaces.
- (2) During takeoff and landing it secures the telescope by pressing it against the axial metal hard stops.

The VIS, shown in Fig. 11, consists of 24 air springs and three dampers. Twelve axial air springs and the three dampers act along the aircraft roll axis, and 12 tangential air springs act in the respective tangential directions on a large circle in the plane of the supporting bulkhead. The position of the inner telescope structure with respect to the bulkhead, also called the VIS position, is measured by seven linear position sensors, two for the vertical and horizontal position, respectively, and three for the axial position of the VIS in the pressure bulkhead. The range of motion of the VIS is ± 15 mm in the

axial direction and ± 10 mm in the other directions before the system encounters one of the axial or tangential hard stops. To control the VIS positions, the air springs are combined into three groups of four air springs for the axial direction and four groups (two groups of four, and two groups of two air springs) for the tangential air springs. Each group can be pressurized individually with dry air from pressure bottles located in the aft compartment on the upper deck.

On the ground and for takeoff and landing, the VIS is usually "centered" and "caged". *Centered* means that the pressure in the tangential air springs is controlled in such a way that the inner part of the VIS is in the center of the pressure bulkhead. *Caged* is the position of the VIS, where the axial air springs are pressurized to 5 bar to push the telescope forward about 15 mm against the axial hard stops. In flight, at an altitude of about 35,000 ft, the VIS is uncaged by lowering the pressure in the axial air springs to about 2.3 bar. The pressure differential between the cabin pressure and the ambient pressure at altitude in the telescope cavity on the other side of the bulkhead causes the telescope to move aft by about 15 mm to the axially centered zero-position.

The VIS is not actively controlled when in caged or uncaged mode. Once the transition between the modes is complete, the system is passive, i.e. the valves to the air springs are closed and neither the pressure in the air springs nor the position of the VIS are controlled. Should pressure variations in the cavity like they occur with changing altitudes require a re-centering of the VIS, a "VIS adjust" command needs to be sent. This starts an automated sequence of position measurements and pressure adjustments of the air springs to move the telescope back to the axial and tangential zero-positions. Since those moves are mostly in translational directions and small rotations are compensated by the Fine Drive, re-centering does not affect the telescope pointing and can be performed while observing. Before landing, the VIS needs to be caged again to secure the telescope and prevent it from moving in the air springs. To cage the VIS, it is centered in the bulkhead plane and the pressure in the three axial groups is increased to 5 bar again, pushing the telescope forward against the hard stops. In case the VIS cannot be fully caged, the remaining 2.3 bar pressure in the axial air springs together with the lower differential pressure at lower altitudes is enough to partially cage the VIS to make the landing safe for the telescope.

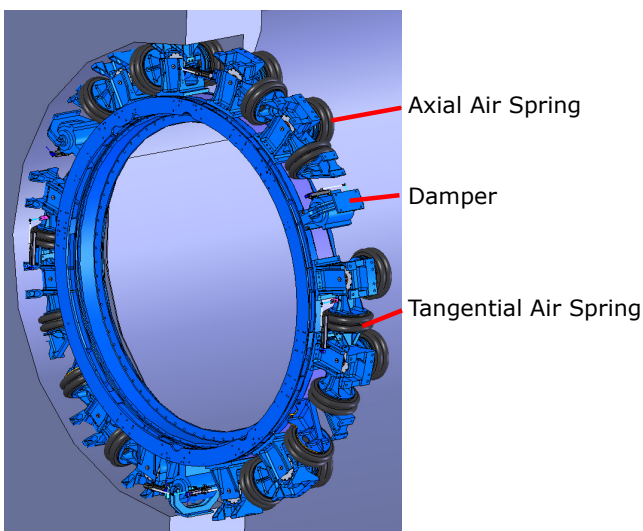


Fig. 11. The vibration isolation system with its axial and tangential airsprings and dampers.

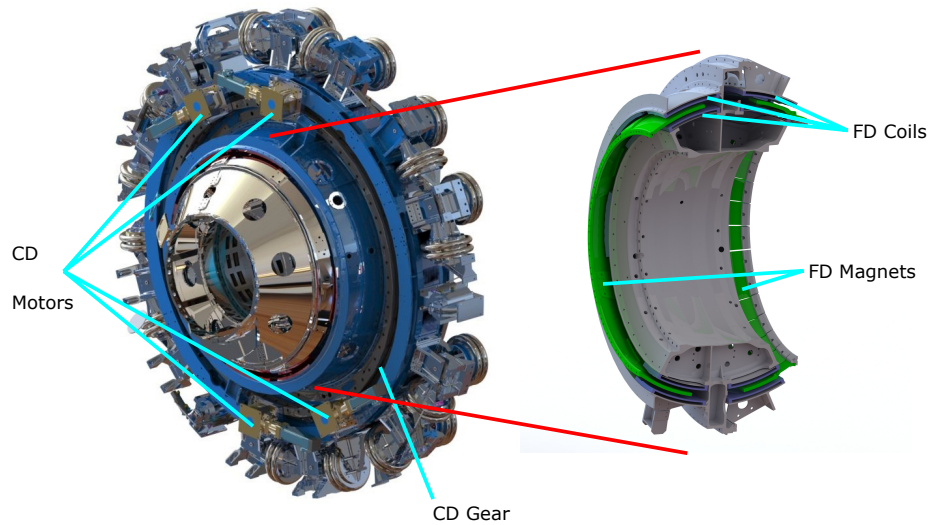


Fig. 12. (Color online) The physically interlaced SUA with the position of the coarse drive motors and gear shown within the VIS on the left side and on the right side the FD motors with the actuator coils shown in purple on the stator carrier and the magnets on the rotor shown in green.

3.2. Coarse drive assembly

The CD moves the telescope in the elevation axis. As depicted in Fig. 12, it resides inside the VIS and consists of a large spur gear, 2.4 m in diameter, that is driven by four electric brushless motors, which connect to the spur gear via planetary/bevel gear boxes. Each motor is capable of producing 4.5 Nm torque. Together with the 3087: 1 combined gear reduction of the planetary/bevel gear and the spur gear, each motor moves the telescope with a torque of > 10 kNm. To eliminate backlash in the gears, the four CD motors are paired and act against each other, two are biased with a positive, and two with a negative torque. Should one motor fail, the other motor in the pair will switch itself off and the remaining two motors rotate the telescope in the so-called degraded mode.

The CD elevation range in flight is limited to $16.5\text{--}68.5^\circ$ by a set of hard stops and bumpers. In case of a malfunction, the CD hard stops are dimensioned such that they can withstand the forces of the telescope hitting the hard stops, while rotation with the maximum possible rate in one direction with the aircraft rolling with the maximum possible roll rate in the other direction. For maintenance purposes, the hard stops can be removed and the telescope can be rotated from 0° to 180° CD elevation.

Usually, the CD is only commanded directly on the ground for tests and maintenance and in flight between two observation legs to get the telescope ready for the next observation. During the observation, the

CD is coupled to the FD and the telescope is stabilized in the inertial reference frame. There are two different coupled modes. In “Coupled Continuous” mode, the CD is actively controlled with a bandwidth of approx. 1 Hz to keep the FD centered in elevation direction. In “Coupled Step” mode, the CD only corrects for FD elevation deflections $> 1.5^\circ$. Standard for observations is the “Coupled Continuous” mode.

The CD motors are equipped with resolvers for commutation and with fail-safe internal brakes that engage when commanded or when the power is removed from the motor. Again, to ensure the safety of the aircraft, the brakes are sized such that they are able to counter the inertia of the telescope even under the worst-case roll acceleration of the aircraft. The CD position is measured by a separate encoder directly on the CD bearing since position measurements on the motor side of the gear are not sufficiently accurate.

3.3. Fine drive assembly

The Fine Drive Assembly actively stabilizes the telescope inertially, i.e. it rejects disturbances acting on the telescope caused by aerodynamic and aeroacoustic loads, residual aircraft motions and vibrations not completely blocked by the VIS, and also disturbances caused by friction of the bearing, seals and cables. Telescope motions like scanning, nodding, etc. are also performed with the FD. Figure 12 depicts the FD’s custom-made double-sided spherical synchronous direct drive motors with permanent

magnets on the rotor structure that connects to the NT.

Two types of sensors are utilized in the system:

- (1) Three custom-made spherical sensors are used for electronic commutation purposes and velocity and motion limit monitoring.
- (2) Three custom-made fiber optic gyroscopes (FOG) determine the inertial attitude of the telescope.

The FD stabilization loop runs with 400 Hz and is constantly active during observations. It allows for $\pm 2.8^\circ$ of motion in all three rotational DoF. Depending on the axis, there are different ways of ensuring that these limits are not exceeded: The CD extends the range in elevation direction. The cross elevation is adjusted to within the FD range by the yaw angle of the aircraft, i.e. the pilots frequently correct course to keep the target in range. None of these background operations affects the ongoing observation because the FD bandwidth exceeds the bandwidth of the CD and the yaw rotation rate of the aircraft. The line of sight axis needs frequent rewinds, depending on the target position in the sky to keep the FD from hitting a limit. Depending on the type of observation, this may or may not interrupt observations.

As a safety measure, the FD motion (in addition to software limits) is limited by hardstops with limit switches. Two pairs of hardstops restrict the motion about the elevation axis and a ring of hardstops restricts the motion about the cross elevation and the line of sight axes to $\pm 3^\circ$. All limit switches are connected in series, so if one switch is triggered, the power to the FD motors and brakes is cut, causing immediate application of the fail-safe brakes. The FD brakes consist of four pairs of pistons that are released with hydraulic pressure provided by the same pump that supplies oil to the hydrostatic bearing. If the pressure in the bearing drops, e.g. due to a hydraulic leak, the brakes close automatically. The brakes are designed to prevent the telescope from moving even under the worst-case pitch, roll and yaw accelerations of the aircraft.

3.3.1. Spherical sensors

The spherical sensors (SPS) measure the angular position of the rotating part of the telescope inside the hydrostatic bearing with respect to the Inner Cradle, which is the structure rotated with the CD. As shown in Fig. 13 it consists of a laser diode with microfocus optics and a Position Sensitive Device

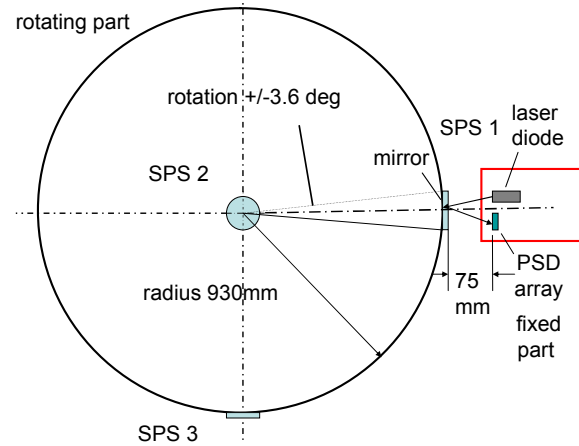


Fig. 13. Layout of the spherical sensors and the spatial distribution of the three units on the hydrostatic bearings circumference.

(PSD) Array attached to the Inner Cradle and a mirror on the rotor structure that reflects the laser to the PSD. Three orthogonally positioned sensors are distributed around the bearing, two in the cavity and one in the cabin.

With these sensors as feedback to the telescope attitude controller, the telescope can be operated in the so-called Local Stabilization Mode, meaning the TA attitude is controlled relative to the aircraft. This mode can be used when the observatory turns to a new heading for the next observation leg or when balancing the telescope before flight.

3.3.2. Fiber optic gyroscopes

During observations the Inertial Stabilization Mode is used to control the telescope. With the FOG measuring the TA angular rates inertially, the telescope is not stabilized with respect to the aircraft but in an inertial reference frame. The aircraft then moves around the telescope, which keeps the astronomical target pinned to its position in the focal plane.

The gyros are mounted on the cabin side, close to the telescope's center of rotation, to minimize temperature effects and the superposition of flexible telescope bending deflections on the rigid body rotation. They were manufactured by the French company IXSEA (now iXblue) with optical fibers with a length of 3,400 m that are arranged as coils with 150 mm diameter. To measure the rotation rate, they make use of the Sagnac effect that can be observed when light from a single source is split to travel in opposite directions along a closed optical path. When this optical path, i.e. the optical fiber

Table 1. Performance values of the FOG 180.

| | |
|-------------------------|---------------------------------|
| Random walk | $0.00022^\circ/\sqrt{\text{h}}$ |
| Bias stability | $0.0007^\circ/\text{h}$ |
| Dynamic range | $\pm 26.3^\circ/\text{s}$ |
| Minimal detectable rate | $0.03 \text{ arcsec}/\text{s}$ |
| Bandwidth | 10 kHz |

coil, rotates, the light waves arrive with a phase difference at the end of the path that is proportional to the angular rate. As described in Harms (2009), performance measurements of the gyros installed in the telescope were executed and basically confirmed the values given by the manufacturer for the so-called FOG 180 system (Faussot *et al.*, 2017) in Table 1.

A new and improved version, the FOG 200, was recently delivered and is currently undergoing first testing with the flight electronics on the aircraft.

3.4. Rotation isolation assembly

The RIA is a hydrostatic bearing that isolates the telescope from aircraft rotations. It consists of the bearing sphere shown in Fig. 14, with a diameter of 1.2 m that is made from cast iron with a bearing surface accuracy of approx. $5 \mu\text{m}$ rms.

The sphere is connected to the NT. The two Bearing Rings connected to the Inner Cradle structure, one on the cavity side and one on the cabin side, are made from steel with bronze-coated sliding surfaces. The nominal oil gap measures approx. $50 \mu\text{m}$.

The oil flow to the bearing is provided by the Oil Supply Unit (OSU) that is located in the cargo bay of the aircraft and provides approximately



Fig. 14. The bearing sphere of the hydrostatic bearing.

50 bar pressure in the supply line. Flow controllers located at the inlets to the bearing reduce this pressure to approximately 15 bar. The oil is routed through multiple filters to prevent larger particles from reaching the bearing and through the Cooling Supply Unit (CSU) for temperature conditioning. The CSU is connected to one of the aircraft's passenger air conditioning heat exchangers. During FD operation, it must be ensured that the oil gap between bearing sphere and rings is kept within the required limits to prevent contact between the two or oil leakage. This means the oil temperature in the bearing must not deviate more than $\pm 1^\circ\text{C}$ from a target temperature derived from the current cabin air temperature. Since the bearing, is part of the pressure boundary between cabin and cavity, the allowable gap size was determined by the maximum pressure difference. Once the oil leaves the bearing, it is collected in two small tanks located on the telescope. When a certain fill level is exceeded, the oil is pumped back into the main reservoir in the cargo bay.

3.5. Balancer drive assembly

The Balancer Drive Assembly is used to move the telescope's center of mass to the center of rotation, i.e. the center of the hydrostatic bearing. Minimizing the imbalance minimizes the FD torque required for keeping the telescope pointed under external static (gravity) and dynamic (maneuver) loads.

When a science instrument is installed, the telescope is balanced roughly by adding or removing steel plates around the telescope's science instrument flange. For precisely balancing the telescope, the Balancer Drive Assembly is available. It consists of four cylindrical housings with 80 kg weights inside that can be moved by 530 mm along a spindle by an electric motor, respectively. One cylinder each is aligned with the cross elevation and the line of sight axis. Two cylinders are aligned with the telescope's elevation axis to improve the balancing capabilities. This setup is required to counter the science instrument's loss of mass due to cryogen boil off over the 10 h mission. When an instrument gets lighter, the weights in the cylinders along the elevation axis are slowly moved forward to balance the science instrument and cabin-part of the telescope with respect to the part in the cavity. Typical balancer speeds depend on the boil-off rate of the instrument and range from 0.0012–0.0037 mm/s. To minimize the torque

required by the FD to keep the telescope pointed, the telescope is fine balanced before each mission.

4. Target Acquisition, Tracking and Scanning

As described in detail in [Temi et al. \(2014\)](#), SOFIA is applying a pointing acquisition method using visible guide stars in the vicinity of the science target to establish the relation of the inertial reference frame to the equatorial reference frame. This is a semi-automatic process wherein the telescope operator is referencing catalog coordinates with centroid positions of stars visible in the guide cameras. With the established blind pointing from aircraft attitude information, a manual star field identification is done usually on the WFI. For higher accuracy, the process then continues on to the FPI. Once the tracking subsystem is provided with the manually identified centroid location and its inertial reference coordinate, the activation of the tracking mode then guarantees that a chosen guide star, and hence the target, is held at the position it was registered to from the catalog. The primary purpose of tracking is to compensate residual gyro drift; it does not respond fast enough to track telescope jitter. A deviation of the centroid in the elevation or cross elevation direction is measured with each new image and, when the exposure conditions allow, the correction is applied to the inertial reference frame. This scheme is passive; images taken during a motion of the telescope like in a nodded observation or by a pending correction are dropped and not considered for tracking until the motion has settled. Tracking is also aware of the ongoing scan motions. This is to avoid a costly synchronization between exposure time and telescope motion commands. The TCM Feed Forward jitter reduction technique (see [Sec. 5.2](#)) keeps the settling phase usually well below one second as locking onto the target is no longer governed by the Fine Drive control loop bandwidth alone. Tracking is maintained during constant linear motion, Lissajous scans or while following a non-sidereal target and is continuously corrected as long as the determination of the centroid can still be guaranteed in the presence of motion streaking. The effect of streaking can be limited by shortening the camera exposure times. Since the timing between camera images and inertial attitude measurements is well known, the pointing accuracy can be maintained at up to 200 arcsec/s.

As acquisition time is critical for the efficient operation, it has been part of the SOFIA design to

utilize automated plate solution techniques. Recently, support of the software Astrometry.net ([Lang et al., 2010](#)) has been added to the mission system. This tool allows execution of the initial blind pointing in a single step with the heading cameras (WFI or FFI). The accuracy is sufficient to directly acquire the desired guide star with the FPI and to start tracking on its centroid.

As a future extension, the acquisition and tracking process can be combined by utilizing the same pattern matching techniques that the Astrometry.net tool is using. This mode is called 3-axis full-frame tracking as opposed to the 2-axis single-centroid tracking mode that is used currently. There, a manual selection of a tracking target is no longer required and is replaced by an automatic selection of available centroids that are then converted into motion invariant hashes and compared against hash tables from e.g. the Gaia Catalog.

4.1. Scanning modes

A new scanning mode was established in 2014 to accommodate the second generation instrument HAWC+ ([Runyon, 2018](#)). It is a 2-axis Lissajous scanning mode to efficiently scan over an area of the sky. The Lissajous pattern is freely configurable. Given that the rates and pointing of the telescope change constantly in this mode, the actual position in the inertial reference frame has to be accurately determined and reported to the science instrument through housekeeping data. Earlier scanning techniques were limited to mostly linear motions and were assumed to run exactly as programmed to avoid polling for housekeeping data at high rates.

5. Pointing Control

The telescope was delivered by the TA Consortium with initial control laws designed and implemented. In the years between delivery and the start of flight testing leading up to initial science flights, great effort was put into improving those initial designs ([Lampater et al., 2010](#); [Lampater, 2014](#)). A modal survey test ([Keas et al., 2010](#)) was performed on the telescope and a considerable amount of instrumentation was attached to the telescope structure for the initial SOFIA flights to comprehensively characterize the structural dynamics of the telescope under disturbance.

While the performed work was highly successful, increasing demand on the pointing stability

requires a continuation of the effort. The pointing stability improvements achieved in recent years and a brief outlook on planned work are summarized in Graf *et al.* (2018a) with more detailed descriptions given in Graf *et al.* (2016, 2017, 2018b).

5.1. Fine drive control

Figure 15 shows the power spectral density of a point source in cross elevation measured with the FPI+. The FD control was active for this test run because aircraft motion or wind loads would push the telescope in a motion limit if the telescope were ever to be operated in open loop mode in flight. To avoid excitation of the many flexible TA structural frequencies shown in this plot, starting at around 20 Hz with the so-called dumbbell mode (flexing of the NT), the FD controller bandwidth is limited to 3–6 Hz, depending on the axis. By using a decoupling matrix, the system is simplified such that three single axis (elevation, cross elevation, line of sight) controllers can be used. Each axis consists of a cascaded controller with an inner velocity loop and an outer position loop. The velocity (rate) is measured by the gyroscopes and integrated to obtain the telescope position (attitude). PID-type controllers are used, more precisely, PI controllers for the velocity loops and PD controllers for the position loops. Notch filter and pole-zero cancellation filter were carefully designed to avoid excitation of the different structural modes in each individual axis. The main design driver was the robustness of the system to guarantee telescope stability under the

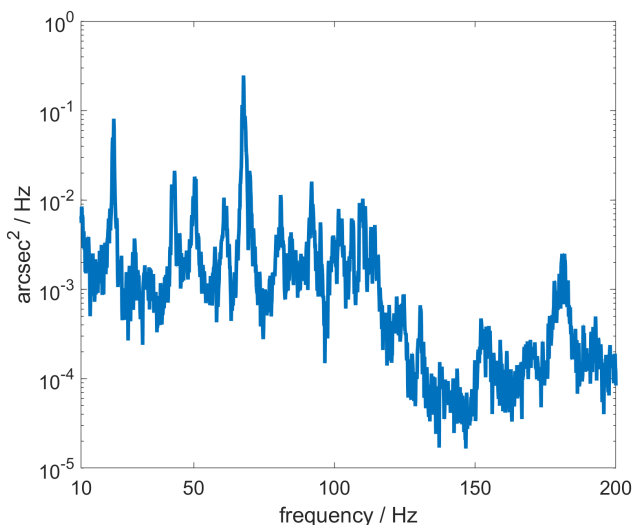


Fig. 15. Power spectral density plot of image motion in cross elevation direction measured with the FPI+.

influence of external disturbances also with slightly changing dynamic properties due to different science instruments mounted to the TA.

5.2. TCM feed forward

Since the FD bandwidth is quite limited, the control deviation, i.e. the difference between desired and actual position is forwarded to the TCM (see TCM Sec. 2.2.2), which has a bandwidth of approximately 50 Hz. The signal is transformed into the SMA coordinate system and filtered with lead-lag filters to reduce phase shift. The TCM then compensates parts of the image motion in the focal plane. This technique is called TCM Feed Forward (TCM FF).

5.3. Flexible body compensation

There are two sets of three one-axis accelerometers mounted to the telescope, one set in the gyro unit, i.e. close to the telescope's center of rotation and center of gravity, and another set at the instrument flange, i.e. close to the focal plane. The acceleration signals from these sensors are used to estimate the image motion resulting from telescope deformations, i.e. flexible telescope modes. This unwanted image motion is then added to the FD control deviation for compensation with FD and TCM. This technique is named the Flexible Body Compensation (FBC).

After initial FBC implementations derived with finite element analysis, there is a more accurate version in use today, which was derived with in-flight measurements. The data required to develop the estimation algorithms are the acceleration measurements and the image motion, which was determined from FPI+ image data recorded with 400 fps. Since the flexible telescope modes are primarily excited through atmospheric turbulence acting on the airframe and the telescope directly, the pilots induce turbulence for these measurements by applying the aircraft's speed-brakes. Naturally, this affects mainly the airframe, it does not produce significant atmospheric turbulence in the telescope cavity. But the excitation of the aircraft translates into telescope motion, which is very similar to the kind experienced under atmospheric turbulence. The application of the speed-brakes is also a rather replicable process, which is very important to compare the measurements done during different parts of a flight or even on different flights.

The impressive effect achieved by activating FBC and TCM FF is illustrated in Fig. 16, which

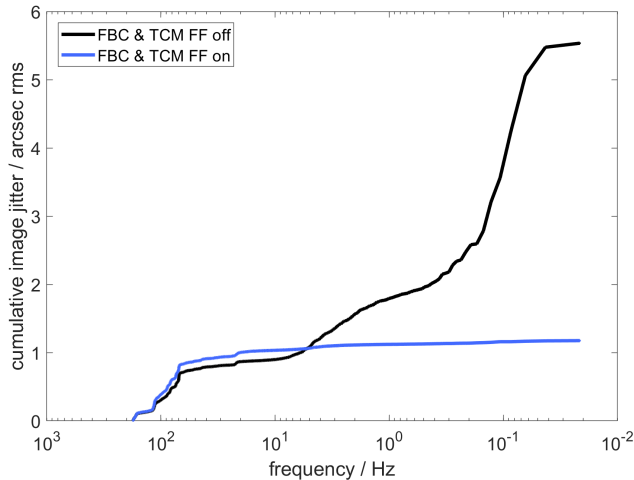


Fig. 16. Reverse cumulative rms plot of imager jitter measured with the FPI+.

compares recorded image jitter with and without these measures activated. It shows the cumulative rms centroid motion of a celestial source measured on a recent flight with the FPI+, logarithmically plotted from high to low frequencies. Activating FBC and TCM FF reduces the image jitter from more than 5.5 arcsec rms to less than 1.2 arcsec rms in this example. This test run was performed in light turbulence. In quiet atmospheric conditions, the image jitter above 1 Hz adds up to approx. 0.8 arcsec rms, which is sufficient to meet the image size requirements given in Sec. 1.

In order to reach SOFIA's image size goals, there is work underway to further improve the FBC system. In addition to an extension of the TCM bandwidth as described in Sec. 2.2 and Lammen *et al.* (2018), additional accelerometers were installed on the three main mirrors. This allows for a more accurate estimation of the image motion. A new FBC algorithm developed with initial data sets recorded with these sensors and the extended TCM bandwidth has been used in simulations to predict the potential for improvement. An additional reduction of image motion of around 25% seems to be a realistic goal for the combination of these improvement efforts (Graf *et al.*, 2018a).

5.4. Active mass dampers

To meet SOFIA's challenging pointing control and image stability goals, additional systems to the telescope's main attitude control system are being studied and implemented. One is the Active Mass Damping (AMD) system designed by Moog CSA

Engineering in collaboration with NASA and DSI (Keas *et al.*, 2012; Janzen & Keas, 2014).

A set of six Reaction Mass Actuators (RMAs) with a rated force output of 45 N (10 lbf) acts on the whiffletree support of the PM. They are driven by a standalone controller independent of the attitude control system. The Multiple Input Multiple Output (MIMO) system simultaneously measures the motion and bending of the PM support by six accelerometers co-located with the actuators. By decomposing the signal into modal coordinates, the control laws used in the damping control system are formulated to act on specific modes of the structure. First implementations of the AMD system focus on two classes of telescope modes:

- (1) Rocking of the PM around the telescope's cross elevation axis at 70 and 73 Hz.
- (2) First bending of the PM at 174 Hz.

Test flights in December 2011 with the AMD system activated showed a significant attenuation of more than 10 dB of telescope vibration at those frequencies. Due to the experimental nature of the system, it was deemed prudent to limit the actuator current during test flights to less than 0.5 A rms which translates to 25% of the system's full power capabilities.

Although the results from the test flights promised significant improvement for image quality, further development of the system stalled due to safety concerns for the PM and other priorities within the program. As those concerns could be addressed and priorities have been rediscussed over time, the AMD system is currently being reactivated by NASA and will be optimized and maintained by DSI for future operational use during SOFIA's science flights. We anticipate a significant contribution to the improvement of image jitter by damping the PM rocking motions. Additionally, damping of internal bending and higher order deformations of the PM is a unique capability of the AMD system, which can not be corrected e.g. by FBC using the fast-steering secondary mirror. Thus, the AMDs are also a prospective measure to address higher-order optical aberrations, such as trefoil and astigmatism, which were identified by SOFIA science instruments to affect image quality (Malicek, 2017).

6. Summary

The SOFIA TA is a sophisticated piece of machinery that needs to maintain accurate pointing while withstanding harsh environmental conditions.

Considering the fact that there was no previous experience in the design, integration and operation of an airborne telescope of this size (the Kuiper Airborne Observatory was significantly smaller), it was a great success that the telescope worked as intended from the very first SOFIA flight and met the initial, so-called early science requirements. The telescope design with its major subsystems is presented in this paper, along with some recent, ongoing and future modifications to further improve the observatory's performance. These modifications include new guide cameras for improved sensitivity, a range of measures to achieve the challenging image size goals including new control algorithms for the telescope main drive, the TCM and the Flexible Body Compensation, an Active Mass Damper system for damping PM deformations and hardware modifications of the TCM to achieve higher bandwidths. New tracking and scanning modes are being worked on to improve the observing efficiency.

In addition, considerable progress has been made in recent years in improving the telescope's reliability, among other things by providing a number of line-replaceable units for various electronic units. The robust design combined with the ongoing performance upgrades and reliability improvements ensure that the telescope will meet and exceed its specifications for the remaining 16 years of its intended lifetime.

Acknowledgments

We thank all personnel and institutions that were and are involved in the SOFIA telescope design and improvement work. We merely introduce the final product of their work. SOFIA, the "Stratospheric Observatory for Infrared Astronomy" is a joint project of the Deutsches Zentrum für Luft- und Raumfahrt e.V. (DLR; German Aerospace Center, grant: 500K0901) and the National Aeronautics and Space Administration (NASA). It is funded on behalf of DLR by the Federal Ministry of Economics and Technology based on legislation by the German Parliament, the state of Baden-Württemberg and the Universität Stuttgart. Scientific operation for Germany is coordinated by the German SOFIA-Institute (DSI) of the Universität Stuttgart, in the USA by the Universities Space Research Association (USRA).

References

Ali, Z. A., Alvarez, P., Cheng, A. *et al.* [2018] "A review of science ground operations for the Stratospheric Observatory

for Infrared Astronomy (SOFIA)," *J. Astron. Instrum.* **7**, 1840002.

Bittner, H., Erdmann, M., Erhard, M. & Haberler, P. [2004] "The optical system of the SOFIA telescope," in *Proc. SPIE*, Vol. 5489, doi: 10.1117/12.551948.

Erdmann, M., Bittner, H. & Haberler, P. [2000] "Development and construction of the optical system for the airborne observatory SOFIA," *Proc. SPIE*, Vol. 4014, doi: 10.1117/12.389107.

Fausso, N., Cottreau, Y., Hardy, G., *et al.* [2017] "Fibre optic gyroscopes for space use," in *Proc. SPIE*, Vol. 10569, doi: 10.1117/12.2307895.

Fruit, M., Antoine, P., Varin, J.-L., Bittner, H. & Erdmann, M. [2003] "Development of the SOFIA silicon carbide secondary mirror," *Proc. SPIE*, Vol. 4857, doi: 10.1117/12.458632.

Graf, F., Reinacher, A., Jakob, H. & Fasoulas, S. [2018a] "Image size and control system developments of the airborne telescope SOFIA," *J. Astron. Instrum.*, in press.

Graf, F., Reinacher, A., Jakob, H. *et al.* [2016] "Pointing and control system performance and improvement strategies for the SOFIA Airborne Telescope," in *Proc. SPIE*, Vol. 9906, doi: 10.1117/12.2231803.

Graf, F., Reinacher, A., Spohr, D., Jakob, H. & Fasoulas, S. [2017] "Simulating SOFIA's image jitter performance and how the results compare to in-flight measurements," in *Proc. SPIE*, Vol. 10401, doi: 10.1117/12.2273453.

Graf, F., Reinacher, A., Reinhart, J. & Fasoulas, S. [2018b] "Design of an innovative observer based feedback enabling faster telescope control in SOFIA," in *Proc. SPIE*, Vol. 10700, doi: 10.1117/12.2306089.

Harms, F. [2009] *A Contribution to Characterizing and Calibrating the Pointing Control System of the SOFIA Telescope*, PhD Thesis, University of Stuttgart.

Harper, D. A., Runyan, M. C., Dowell, C. D. *et al.* [2018] "The HAWC+ far infrared camera and polarimeter for SOFIA," *J. Astron. Instrum.* **7**, 1840008.

Janzen, P. & Keas, P. [2014] "Implementation of an active vibration damping system for the SOFIA telescope assembly," *Proc. SPIE*, Vol. 9145, doi: 10.1117/12.2056861.

Kaercher, H. J., Kunz, N., Temi, P. *et al.* [2014] "SOFIA pointing history," in *Proc. SPIE*, Vol. 9145, doi: 10.1117/12.2055463.

Kaercher, H. J., Erickson, E. F., Krabbe, A. & Wagner, J. [2016] "SOFIA Design History," in *Proc. SPIE*, Vol. 9906, doi: 10.1117/12.2232715.

Keas, P., Dunham, E., Lampater, U. *et al.* [2012] "Active damping of the SOFIA telescope assembly," in *Proc. SPIE*, Vol. 8444, doi: 10.1117/12.924791.

Keas, P., Brewster, R., Guerra, J. *et al.* [2010] "SOFIA telescope modal survey test and test-model correlation," in *Proc. SPIE*, Vol. 7738, doi: 10.1117/12.856507.

Lachenmann, M., Wolf, J., Strecker, R. *et al.* [2014] "Environmental testing for new SOFIA flight hardware," in *Proc. SPIE*, Vol. 9145, doi: 10.1117/12.2056976.

Lammen, Y., Reinacher, A., Greiner, B., Wagner, J. & Krabbe, A. [2018] "Increasing the SOFIA secondary mirror mechanism's fast steering capability by identification of a structural resonance and its subsequent elimination through mass re-distribution," *J. Astron. Instrum.* **7**, 1840001

Lammen, Y., Reinacher, A., Kjølberg, I. *et al.* [2016] "SOFIA secondary mirror mechanism heavy maintenance and

- improvements,” in *Proc. SPIE*, Vol. 9906, doi: 10.1117/12.2231352.
- Lampater, U., Herter, T., Keas, P. et al. [2010] “Preparation of the pointing and control system of the SOFIA airborne telescope for early science missions,” in *Proc. SPIE*, Vol. 7733, doi: 10.1117/12.856562.
- Lampater, U. [2014] *Improvements to the Image Stability of the SOFIA Airborne Telescope* PhD Thesis, University of Stuttgart.
- Lang, D., Hogg, D., Mierle, K., Blanton, M. & Roweis, S. [2010] “Astrometry.net: Blind astrometric calibration of arbitrary astronomical images,” *AJ* **139**, 1782.
- Malicek, B. [2017] *Investigation of Optical Aberration Due to Deformations of the SOFIA Primary Mirror Assembly* Bachelor Thesis, University of Stuttgart.
- Pfüller, E., Wolf, J. & Wiedemann, M. [2018] “The SOFIA Focal Plane Imager: A highly sensitive and fast photometer for the wavelength range 0.4 to 1 micron,” *J. Astron. Instrum.* **7**, 1840006
- Reinacher, A., Lammen, Y., Graf, F. & Jakob, H. [2016a] “SOFIA pointing and chopping: Performance and prospect,” in *Proc. SPIE*, Vol. 9973, doi: 10.1117/12.2237789.
- Reinacher, A. [2014] *Inflight Commissioning and Performance Improvement of the SOFIA Secondary Mirror Mechanism*, PhD Thesis, University of Stuttgart.
- Reinacher, A., Onillon, E. & Roeser, H.-P. [2010] “Improvement of the SOFIA secondary mirror controller,” in *Proc. SPIE*, Vol. 7733, doi: 10.1117/12.856554.
- Reinacher, A. & Roeser, H.-P. [2011] “Modeling of the SOFIA secondary mirror controller,” in *Proc. SPIE*, Vol. 8336, doi: 10.1117/12.915590.
- Reinacher, A., Lammen, Y. & Roeser, H.-P. [2016b] “SOFIA’s secondary mirror assembly: In-flight performance and control approach,” *Proc. SPIE*, Vol. 9908, doi: 10.1117/12.2232851.
- Stoeffler, G. & Heydenreich, R. [2000] “Bearing sphere for SOFIA telescope: A challenge for design and manufacturing,” in *Proc. SPIE*, Vol. 4014, doi: 10.1117/12.389110.
- Sust, E., Weis, U., Bremers, E. & Schubbach, W. [2003] “Manufacturing and integration of the SOFIA suspension assembly,” in *Proc. SPIE*, Vol. 4857, doi: 10.1117/12.458583.
- Temi, P., Marcum, P., Young, E. et al. [2014] “The SOFIA observatory at the start of routine science operations: Mission capabilities and performance,” *ApJS* **212**, 24, doi: 10.1088/0067-0049/212/2/24.
- Wandner, K. [2003] “The Telescope control system of SOFIA,” in *Proc. SPIE*, Vol. 4857, doi: 10.1117/12.458582.
- Wiedemann, M., Wolf, J., McGrotty, P., Edwards, C. & Krabbe, A. [2016] “A high-sensitivity EM-CCD camera for the open port telescope cavity of SOFIA,” in *Proc. SPIE*, Vol. 9906, doi: 10.1117/12.2231809.
- Wolf, J., Colditz, S., Lachenmann, M. et al. [2016] “Deutsches SOFIA Institut (DSI) at the SOFIA Science Center: Engineering and scientific contributions to the airborne observatory,” in *Proc. SPIE*, Vol. 9973, doi: 10.1117/12.2237207.